Journal of Biomolecular NMR, 9 (1997) 409–422

J-Bio NMR 428

Pulse schemes for the measurement of $^3J_{C'C^\gamma}$ and $^3J_{NC^\gamma}$ scalar couplings in ^{15}N,^{13}C uniformly labeled proteins

Robert Konrat*, D.R. Muhandiram, N.A. Farrow and Lewis E. Kay

Protein Engineering Network of Centres of Excellence and Departments of Medical Genetics, Biochemistry and Chemistry, University of Toronto, 1 Kings College Circle, Toronto, ON, Canada M5S 1A8

Received 18 November 1996
Accepted 7 January 1997

Keywords: Triple-resonance NMR; Quantitative J spectroscopy; $^3J_{C'C^\gamma}$ and $^3J_{NC^\gamma}$ scalar couplings; χ_1 dihedral angle

Summary

Pulse sequences are presented for the measurement of $^3J_{C'C^\gamma}$ and $^3J_{NC^\gamma}$ scalar couplings for all C^γ containing residues in ^{15}N,^{13}C uniformly labeled proteins. The methods described are based on quantitative J correlation spectroscopy pioneered by Bax and co-workers [Bax et al. (1994) *Methods Enzymol.*, **239**, 79–105]. The combination of $^3J_{C'C^\gamma}$ and $^3J_{NC^\gamma}$ scalar coupling constants allows the assignment of discrete rotameric states about the χ_1 torsion angle in cases where such states exist or, alternatively, facilitates the establishment of noncanonical χ_1 conformations or the presence of rotameric averaging. The methods are applied to a 1.5 mM sample of staphylococcal nuclease.

Introduction

Molecular structure determination by NMR is based to a large extent on the use of ^1H-^1H distance restraints established by the nuclear Overhauser effect (NOE) and on torsion angle restraints provided by the measurement of homo- and heteronuclear scalar coupling constants (Bystrov, 1976; Wüthrich, 1986). In the case of macromolecular applications, NOEs are most conveniently measured by recording three- and four-dimensional heteronuclear experiments with resolution achieved by measuring the chemical shifts of heteroatoms to which the proximal protons are attached (Clore and Gronenborn, 1991; Bax and Grzesiek, 1993). Recently, a large number of methods have been developed for measuring scalar couplings (Bax et al., 1994; Biamonti et al., 1994); such couplings can be related to torsion angles through Karplus-type relationships (Karplus, 1959). These methods include experiments based on the E.COSY principle (Griesinger et al., 1986) where, in the case of spins A and B scalar coupled to a mutual coupling partner C, it is possible to measure couplings, J_{BC}, which are smaller than the line widths of spins A and B so long as the multiplet components are well separated by J_{AC}. The values of J_{BC} obtained using this approach must be corrected for the spin flips of spin C which occur during the interval between the transfer of magnetization from A to B (Harbison, 1993). An alternative strategy called quantitative J analysis allows the measurement of couplings by allowing magnetization to be transferred between coupled spins A and B and quantitating the extent of transfer, related to J_{AB}, through the measurement of intensities of cross (ω_A, ω_B) and diagonal peaks (ω_A,ω_A). Bax and co-workers have developed a large suite of experiments based on the quantitative J principle to measure both homo- and heteronuclear couplings (Bax et al., 1994) and have presented parameterized Karplus equations to facilitate the conversion of measured J values to the appropriate dihedral angles (Vuister and Bax, 1993; Wang and Bax, 1995). The majority of the methods developed to date have focused on the measurement of couplings to define backbone torsion angles or side-chain torsions involving a select number of residues (Schwalbe et al., 1993; Vuister et al., 1993; Karimi-Nejad et al., 1994; Hu and Bax, 1996).

Interest in the development of methods to measure scalar couplings in our laboratory has been stimulated by our studies of unfolded or partially unfolded states of proteins and attempts to characterize structure in such

*Present address: Institute of Organic Chemistry, University of Innsbruck, Innrain 52A, A-6060 Innsbruck, Austria.

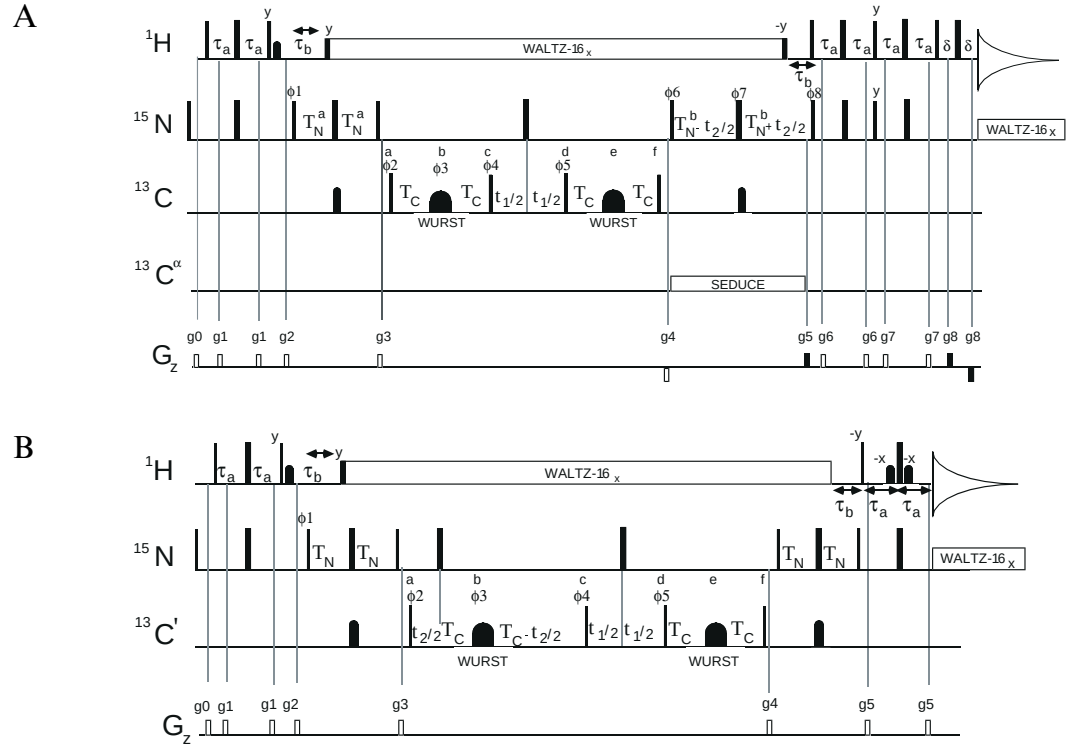

Fig. 1. Pulse schemes for measuring $^3J_{C'C\gamma}$. All narrow (wide) pulses have flip angles of 90° (180°) and are applied along the x-axis, unless indicated otherwise. The ^1H, ^{15}N, ^{13}C and $^{13}C^{\alpha}$ carriers are centered at 4.7 (water), 119, 101 and 58 ppm, respectively. Decoupling is interrupted prior to the application of gradient pulses (Kay, 1993). Proton pulses are applied using a 27 kHz rf field with the exception of the 2 ms rectangular water-selective 90° pulse applied during the initial INEPT (Morris and Freeman, 1979) transfer ($^1H \rightarrow {}^{15}N$), the 6.6 kHz WALTZ-16 (Shaka et al., 1983) decoupling pulses (applied along the ±x-axes) and the 6.6 kHz 90° ±y pulses flanking the WALTZ decoupling interval. The ^{15}N pulses are at a field of 6.1 kHz and WALTZ-16 decoupling during acquisition is applied with a 1 kHz field. The first and last ^{13}C pulses are G3 inversion pulses (Emsley and Bodenhausen, 1992) of duration 450 μs, with the center of excitation shifted to 176 ppm by 75 ppm phase modulation (Boyd and Soffe, 1989; Patt, 1992) of the first pulse (carrier at 101 ppm) and 118 ppm modulation of the second pulse (carrier at 58 ppm, Fig. 1A) or 75 ppm phase modulation of the second pulse (carrier at 101 ppm, Fig. 1B). All ^{13}C 90° pulses are applied with a 21 kHz field; the pulses at points a and f are phase modulated by 75 ppm so that the center of excitation is at 176 ppm. The ^{13}C pulses of phases ϕ4 and ϕ5 are applied at 101 ppm, approximately equidistant from the C' and aliphatic C^{γ} spectral regions. The WURST pulses (Kupce and Freeman, 1995) at points b and e in the sequence are of duration 500 μs, with the center of the 80 kHz frequency sweep set at 176 ppm. The first and last 30% of each pulse was ramped from 0 to 10 kHz with a ramping profile having the shape of a sine function. The amplitude of each WURST pulse was maintained at 10 kHz for the middle 40% of each pulse. The phases of the WURST pulses were adjusted so that all of the signal was present in only one of the channels for $t_2 = 0$ in the case of sequence B and these phases were employed in scheme A. The delays employed are: $\tau_a = 2.4$ ms, $\tau_b = 5.5$ ms, $T_N = T_N^a = 13.5$ ms, $T_N^b = 15.0$ ms, $T_C = 28.4$ ms and $\delta = 0.5$ ms. (A) Cross and diagonal peaks are observed at $[\omega_{C'}(i),\omega_N(i+1),\omega_{NH}(i+1)]$ and $[\omega_{C'}(i),\omega_N(i+1),\omega_{NH}(i+1)]$, respectively. After point f the carbon carrier is jumped to 58 ppm for the duration of the sequence. On-resonance $^{13}C^{\alpha}$ WALTZ decoupling employing pulses having the SEDUCE-1 (McCoy and Mueller, 1992) profile (315 μs) is applied during t_2 evolution. The phase cycling used is: ϕ1 = (x,–x); ϕ2 = x; ϕ3 = 2(x),2(y),2(–x),2(–y); ϕ4 = 8(y),8(–y); ϕ5 = (y,–y); ϕ6 = x; ϕ7 = 4(x),4(–x); ϕ8 = x; acq = (x,–x,–x,x). Quadrature in F1 is obtained by States-TPPI (Marion et al., 1989b) of ϕ2, ϕ3 and ϕ4. Quadrature in F2 is obtained by inverting the phase of the gradient g5 and adding 180° to the phase ϕ8, as described previously in the literature (Kay et al., 1992). The phase ϕ6 and the phase of the receiver are incremented by 180° for each value of t_2. The durations and strengths of the gradients are: g0 = (0.5 ms, 8 G/cm), g1 = (0.4 ms, 4 G/cm), g2 = (1 ms, 10 G/cm), g3 = (1 ms, 6 G/cm), g4 = (1 ms, –25 G/cm), g5 = (1.25 ms, 30 G/cm), g6 = (0.2 ms, 3 G/cm), g7 = (0.3 ms, 1.5 G/cm), g8 = (0.125 ms, 14.5 G/cm). Coherence transfer selection gradients are indicated by shaded rectangles. (B) Cross and diagonal peaks are observed at $[\omega_{C\gamma}(i),\omega_{C'}(i),\omega_{NH}(i+1)]$ and $[\omega_{C'}(i),\omega_{C'}(i),\omega_{NH}(i+1)]$, respectively. The phase cycling employed is identical to that described above with quadrature in F1 obtained by States-TPPI (Marion et al., 1989b) of ϕ2, ϕ3 and ϕ4, as before. The carbon carrier is maintained at 101 ppm throughout the sequence. Quadrature in F2 is obtained by States-TPPI of ϕ2. The durations and strengths of the gradients are: g0 = (0.5 ms, 8 G/cm), g1 = (0.4 ms, 4 G/cm), g2 = (1 ms, 10 G/cm), g3 = (1 ms, 6 G/cm), g4 = (0.5 ms, 7.5 G/cm), g5 = (0.25 ms, 20 G/cm).

molecules (Zhang and Forman-Kay, 1995; Zhang et al., 1997). To this end, we have recently developed a suite of NOE-based experiments in which backbone ^{15}N or carbonyl ($^{13}C'$) chemical shifts are recorded to help assign aliphatic-NH and aliphatic-aliphatic NOEs (Zhang et al., 1997). However, the interpretation of NOE intensities in unfolded protein states is severely compromised by the time-dependent modulation of interproton distances. In this regard, additional information provided through the measurement of scalar couplings would be useful. With this in mind, we have developed pulse schemes for the measurement of $^{13}C'$-$^{13}C^{\gamma}$ and ^{15}N-$^{13}C^{\gamma}$ scalar couplings. In combination, $^3J_{C'C\gamma}$ and $^3J_{NC\gamma}$ can define the χ_1 rotameric state of an amino acid or, at the very least, establish that

either the χ_1 torsion angle of a particular side chain exists in a noncanonical conformation or that χ_1 averaging is present. In principle, couplings between other combinations of nuclei, including $^3J_{H^\alpha H^\beta}$ (Eggenberger et al., 1992; Emerson and Montelione, 1992; Grzesiek et al., 1995), $^3J_{NH^\beta}$ (Archer et al., 1991) and $^3J_{C'H^\beta}$ (Eggenberger et al., 1992; Grzesiek et al., 1992; Schmidt et al., 1996), can also be measured to provide additional sources of information on χ_1. However, the H^β protons are often degenerate in unfolded proteins, complicating the analysis of these couplings in terms of either a defined rotameric state or averaging between states. We therefore focus on the measurement of $^3J_{NC^\gamma}$ and $^3J_{C'C^\gamma}$ in the present manuscript and illustrate the methods on a sample of staphylococcal nuclease.

Materials and Methods

A 1.5 mM sample of staphylococcal nuclease (SNase) complexed with Ca^{2+} and pdTp and uniformly ^{15}N,^{13}C labeled was prepared as described previously (Nicholson et al., 1992). All spectra were recorded on a Varian UNITY+ 500 MHz spectrometer equipped with a pulsed field gradient unit and an actively shielded triple-resonance probe head. A temperature of 35 °C was employed in all experiments. In the case of the HNCOC$^\gamma$ experiment (Fig. 1A) spectral widths of 5834 (^{13}C), 1650 (^{15}N) and 8000 Hz (NH) were recorded in each of F1, F2 and F3, with acquisition times of 8.2, 31.5 and 64.0 ms in each of t_1, t_2 and t_3. Identical F1(t_1) and F3(t_3) spectral widths and (acquisition times) were recorded in the HNCOC$^\gamma$ and H(N)COC$^\gamma$ (Fig. 1B) experiments; however, a spectral width of 1169 Hz (C') was employed in F2 in H(N)COC$^\gamma$ and an acquisition time of 54.8 ms was used. Spectral widths of 1650 (^{15}N, 50.9 ms), 5155 (^{13}C, 6.2 ms) and 8000 Hz (NH, 64.0 ms) were recorded in the HNC$^\gamma$ experiment (Fig. 2A), while the corresponding values were 1650 (^{15}N, 50.9 ms), 1500 ($^{13}C'$, 21.3 ms) and 8000 Hz (NH, 64.0 ms) for HNCO (Fig. 2B). A repetition delay of 1 s was used between scans, giving rise to a total measuring time for each experiment of between 2 and 2.5 days.

The data sets were processed using nmrPipe/nmrDraw software and analyzed using routines in the nmrPipe software (Delaglio et al., 1995) kindly provided by Frank Delaglio, NIH (Bethesda, MD, U.S.A.). In the NH dimension of all data sets a solvent suppression filter was employed to minimize distortions from the residual water (Marion et al., 1989a) prior to apodization with a Lorentzian-to-Gaussian window function. The data were zero filled to twice the size and Fourier transformed, retaining only the NH region of the spectrum. In the case of data sets generated from the sequences of Fig. 1, the t_1 dimensions were apodized with Lorentzian-to-Gaussian window functions and zero filled to 128 complex points prior to Fourier transformation. Mirror image linear prediction (Zhu and Bax, 1990) was used to extend the t_2 time domain data by a factor of 2 prior to Lorentzian-to-Gaussian apodization, followed by zero filling to 256 complex points and subsequent Fourier transformation. In the case of the HNCO and HNC$^\gamma$ experiments the carbon dimensions were zero filled twice, while the ^{15}N dimensions were zero filled from 84 to 256 complex points. Other details are as described for the HNCOC$^\gamma$/H(N)COC$^\gamma$ experiments. The final sizes of the data matrices (real points) were F1: 128, F2: 256, F3: 308 for the HNCOC$^\gamma$/H(N)COC$^\gamma$ and F1: 256, F2: 128, F3: 308 for the HNCO/HNC$^\gamma$ experiments. (Note that F1 and F2 are interchanged in the two sets of experiments; see Figs. 1 and 2.)

Results and Discussion

Experiments for measuring $^3J_{C'C^\gamma}$

Figure 1 illustrates the HNCOC$^\gamma$ and H(N)COC$^\gamma$ pulse schemes for measuring C'-C$^\gamma$ couplings. In the first sequence (Fig. 1A), magnetization originating on the NH spin of residue (i+1) is transferred to the C' spin of the preceding residue via the large one-bond NH-^{15}N and ^{15}N-$^{13}C'$ couplings. Subsequently, transverse C' magnetization, established by the carbon pulse of phase $\phi 2$, is allowed to evolve for a period of $2T_C$ (see below). During this delay a fraction of the magnetization proportional to $\cos(2\pi\, ^3J_{C'C^\gamma} T_C)$ remains on the carbonyl spin, while a fraction proportional to $\sin(2\pi\, ^3J_{C'C^\gamma} T_C)$ is transferred to the C$^\gamma$ spin. After evolution of carbon magnetization during t_1, the signal from both C$^\gamma$ and carbonyl spins is transferred back to the site of origination following the reverse of the original pathway. Fourier transformation of the resulting 3D data set gives peaks centered at $[\omega_{C^\gamma}(i),\omega_N(i+1),\omega_{NH}(i+1)]$ and at $[\omega_{C'}(i),\omega_N(i+1),\omega_{NH}(i+1)]$, referred to as cross and diagonal peaks, respectively. Because magnetization evolves in a similar manner during the transfer steps both before and after the t_1 period, the intensity ratio of the cross and diagonal peaks is given by $-\tan^2(2\pi\, ^3J_{C'C^\gamma} T_C)$. The transfer pathway in the present experiment is summarized by

$$\begin{aligned} &\mathrm{NH} \xrightarrow{J_{NH}} {}^{15}\mathrm{N} \xrightarrow{J_{NC'}} {}^{13}\mathrm{C}' \xrightarrow{{}^3J_{C'C^\gamma}} {}^{13}\mathrm{C}^\gamma, {}^{13}\mathrm{C}'(t_1) \\ &\xrightarrow{{}^3J_{C'C^\gamma}} {}^{13}\mathrm{C}' \xrightarrow{J_{NC'}} {}^{15}\mathrm{N}(t_2) \xrightarrow{J_{NH}} \mathrm{NH}(t_3) \end{aligned} \qquad (1)$$

where t_i are acquisition times and the couplings of interest are indicated above the arrows. In what follows, the superscript '3' in $^3J_{C'C^\gamma}$ will be omitted. Note that the delay $2T_C$ is set to $\approx 3/J_{C'C^\alpha}$, ensuring that (i) C'-C$^\alpha$ correlations which are not of interest in the present experiment are minimized, thereby increasing the sensitivity of C'-C$^\gamma$ cross peaks; and (ii) a sufficient time is allowed for the establishment of correlations arising from $J_{C'C^\gamma}$.

The flow of magnetization in a related experiment designed for the measurement of ^{13}C-^{13}C J couplings between carbonyl and carbonyl/carboxyl carbons has been

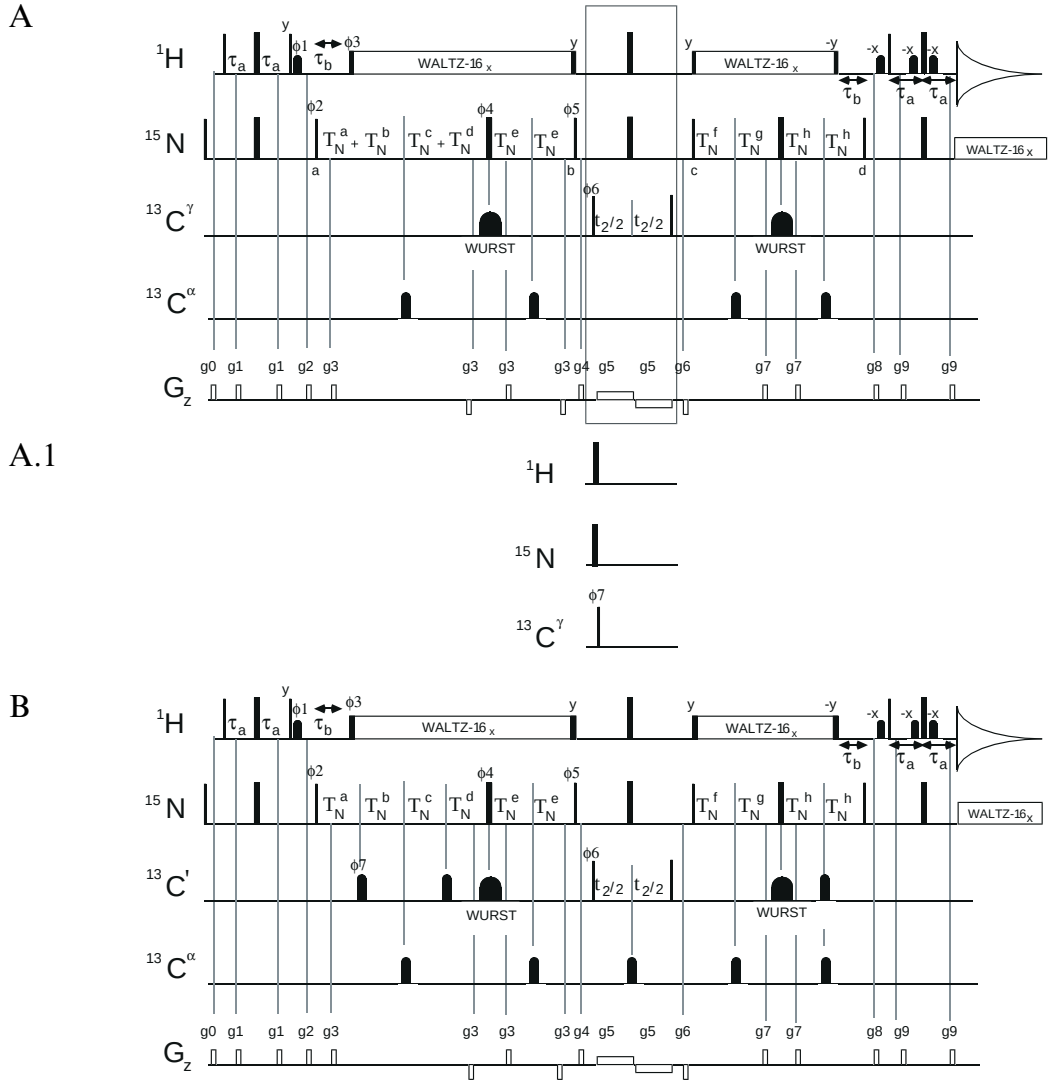

Fig. 2. (A) HNC$^{\gamma}$ pulse scheme. Many of the details of this sequence are described in the legend to Fig. 1 and only the differences are indicated here. In the present application the ^{13}C carrier was positioned at 101 ppm and the center of the frequency sweep of the WURST pulses (Kupce and Freeman, 1995) is at 176 ppm. All $^{13}C^{\alpha}$ pulses are 1.5 ms I-BURP-2 inversion pulses (Geen and Freeman, 1991) with the center of excitation at 57 ppm and are applied using a 44 ppm phase-shifted rf field. The delays employed are: $\tau_a = 2.4$ ms, $\tau_b = 5.5$ ms, $T_N^a = T_N/4 + t_1/4 + \gamma/2$, $T_N^b = T_N/4 + \gamma/2$, $T_N^c = T_N/4 - \gamma/2$, $T_N^d = T_N/4 + t_1/4 - \gamma/2$, $T_N^e = T_N/2 - t_1/4$, $T_N^f = T_N/2 + \gamma$, $T_N^g = T_N/2 - \gamma$, $T_N^h = T_N/2$, $T_N = 33.3$ ms. Note that most of the delays on each of the ^{15}N lines of schemes A and B extend either from a ^{15}N pulse or to a ^{15}N pulse, so that the delay $T_N^c + T_N^d$ of scheme A, for example, extends from the center of the first $^{13}C^{\alpha}$ inversion pulse to the ^{15}N pulse of phase $\phi4$. During the interval from a to b and from c to d the evolution of nitrogen magnetization due to ^{15}N-$^{13}C^{\alpha}$ scalar couplings should be refocused for maximum sensitivity. The WURST pulses do not invert all ^{13}C spins simultaneously (see text); in the present application an 80 kHz sweep (40 kHz downfield of the carbonyl region to 40 kHz upfield) is employed. The ^{13}C' and ^{15}N spins are inverted simultaneously and the $^{13}C^{\alpha}$ spins are inverted a time ε later. The delay γ is set according to the relation $\gamma = -\varepsilon$, with ε set to 92 and 111 μs at 500 and 600 MHz, respectively (500 μs WURST inversion pulse). A flip-back (Grzesiek and Bax, 1993) WATERGATE scheme (Piotto et al., 1992) is employed at the end of each sequence. The phase cycling employed is: $\phi1 = 8(x),8(-x)$; $\phi2 = x$; $\phi3 = 8(y),8(-y)$; $\phi4 = 4(x),4(y),4(-x),4(-y)$; $\phi5 = (x,-x)$; $\phi6 = 2(x),2(-x)$; acq = x,2(–x),x,–x,2(x),–x. Quadrature in F1 and F2 is obtained by States-TPPI (Marion et al., 1989b) of $\phi2$ and $\phi6$, respectively. The durations and strengths of the gradients are: g0 = (0.5 ms, 7.5 G/cm), g1 = (0.2 ms, 3 G/cm), g2 = (1 ms, 20 G/cm), g3 = (0.3 ms, 20 G/cm), g4 = (1 ms, 6 G/cm), g5 = (t_2/2, 2 G/cm), g6 = (1 ms, –25 G/cm), g7 = (0.4 ms, 20 G/cm), g8 = (0.3 ms, 10 G/cm), g9 = (0.3 ms, 15 G/cm). (A.1) Scheme to record the 2D ^{1}H-^{15}N 'diagonal' spectrum. The pulses in the boxed region in A are replaced by the scheme indicated in A.1. All details are as in A with the exception that $\phi5 = (y,-y)$, the phase of the ^{15}N pulse at point d is y, $\phi7 = 2(x),2(-x)$ and acq = x,–x,x,2(–x),x,–x,x. (B) HNCO pulse scheme. Details are as in A with the exception that the carbon carrier is jumped from 101 to 176 ppm immediately after application of gradient g4 and returned to 101 ppm prior to g6. The $^{13}C^{\alpha}$ 180° inversion pulse applied in the center of t_2 has a G3 profile (285 μs) and is phase modulated by 136 ppm (i.e., the center of excitation is at 40 ppm). The ^{13}C' 90° pulses bracketing the t_2 period are applied at a field strength of 21 kHz while the first two and the last ^{13}C' pulses are 1.5 ms I-BURP-2 inversion pulses centered at 176 ppm. The ^{13}C' and $^{13}C^{\alpha}$ inversion pulses in the center of the $2T_N^h$ period are applied simultaneously by constructing a waveform which consists of the sum of the individual waveforms and adding 6 dB to the voltage level for the pulse. The phase $\phi7$ is cycled (x,–x). *Scheme for measuring* $1/T_1(N_zC_z^{\gamma})$. In the scheme of Fig. 2A the pulses in the boxed region are eliminated and the phase cycle is: $\phi1 = 4(x),4(-x)$; $\phi2 = x$; $\phi3 = 4(y),4(-y)$; $\phi4 = 2(x),2(y),2(-x),2(-y)$; $\phi5 = (x,-x)$; acq = x,–x,–x,x. After point b the signal of interest is of the form $N_zC_z^{\gamma}$ and is allowed to relax for a delay T. Magnetization is subsequently transferred back to the point of origination with pulses starting at point c. ^{1}H decoupling is applied during T.

described previously by Hu and Bax (1996); however, a number of important differences between this sequence and the ones presented here are worthy of mention. Although we will focus exclusively on the measurement of three-bond couplings established by correlations connecting intraresidue C' and C^{γ} spins, the present scheme also allows the measurement of three-bond C'-C' couplings as well as interresidue three-bond C'-C^{β} couplings. Because of the 160 ppm chemical shift dispersion of C^{γ} carbons ($\delta_{C\gamma}$ of Asx ≈180 ppm, $\delta_{C\gamma}$ for aromatic residues ≈130 ppm and $\delta_{C\gamma}$ of aliphatic amino acids ranges from 40 to 20 ppm), care must be taken in the choice of inversion pulses (applied at points b and e in the sequences of Fig. 1) so that the complete range of C^{γ} carbons can be inverted properly. To this end, WURST pulses (Kupce and Freeman, 1995) of duration 500 μs and with a linear frequency sweep of 80 kHz are employed (see the legend to Fig. 1 for details); these pulses have an inversion bandwidth of ±24.5 kHz (>98% inversion), sufficient to cover the wide C^{γ} carbon chemical shift range.

In the context of these experiments the WURST pulses must also refocus transverse backbone carbonyl magnetization during each of the $2T_C$ periods. Although WURST pulses were not designed with the refocusing of transverse magnetization in mind, simulations indicate that for a bandwidth of ±23.5 kHz centered about the midpoint of the frequency sweep, over 98% of the transverse magnetization that was present before the pulse is retained in the x-y plane after the pulse. However, simulations of the effects of these pulses on transverse magnetization indicate that the phase versus frequency profile is quadratic, with a minimum located at the center of the sweep. The center of the sweep of each WURST pulse is, therefore, set to the middle of the carbonyl region of the carbon spectrum (176 ppm) and, because of the small C' chemical shift dispersion, the phase error introduced by these pulses is very small. Simulations indicate that the phase changes by less than 1.5° over a range of ±750 Hz centered in the middle of the frequency sweep. These pulses are thus extremely well suited for the present application.

The effects of a WURST pulse on a $^{13}C'$-$^{13}C^{\gamma}$ two-spin system can be well approximated by assuming that inversion for a given spin occurs at its resonance condition (Bohlen et al., 1989). That is, during a frequency sweep a spin is inverted at the point when the frequency of the pulse coincides with the resonance frequency of the spin. Thus, it is clear that different $^{13}C^{\gamma}$ spins will be inverted at different times during the pulse in a manner dependent on their offset. It is straightforward to show that evolution of $^{13}C'$ magnetization due to $J_{C'C\gamma}$ will occur for a time of $2T_C + \tau_p^W - 2\zeta$ between points a and c or d and f in Fig. 1, where τ_p^W is the duration of the WURST pulse and ζ is the time that it takes the pulse to sweep from the C' chemical shift region of the carbon spectrum to the chemical shift of the $^{13}C^{\gamma}$ in question. Because τ_p^W is small (500 μs) and a large frequency sweep is employed (80 kHz), $2T_C + \tau_p^W - 2\zeta \approx 2T_C + \tau_p^W$; in any event, ζ is easily calculated for each C^{γ} chemical shift.

As described above, the pulse schemes of Fig. 1 allow the measurement of $^{13}C'$-$^{13}C^{\gamma}$ couplings for *all* C^{γ} containing residues and, because of the large dispersion of $^{13}C^{\gamma}$ chemical shifts, an evaluation of potential errors introduced by off-resonance effects of the carbon pulses is in order. All carbon pulses, with the exception of the ^{13}C 90° pulses bracketing the t_1 evolution period, are applied as 'on-resonance' pulses. For example, although the carbon carrier is centered at 101 ppm throughout the experiment, approximately equidistant from C' and aliphatic C^{γ} chemical shifts, the ^{13}C 90° pulses at points a and f in the sequences of Fig. 1 and the first and last 180° pulses (shaped) are phase modulated (Boyd and Soffe, 1989; Patt, 1992) with the center of excitation in the middle of the carbonyl region. In contrast, however, the carbon 90° pulses immediately surrounding t_1 must excite both C' and C^{γ} spins and are therefore best applied with the center of excitation at 101 ppm. We have analyzed the effects of these off-resonance pulses in some detail (see the Appendix) and conclude that, for the highest values of carbon rf fields currently available (~21 kHz) and for offsets as large as 10 or 11 kHz, errors of any significance are not introduced into the measured couplings, although the intensities of cross and diagonal peaks used to establish the J values are reduced somewhat (see the Appendix).

Figure 1B illustrates a second pulse sequence for measuring $J_{C'C\gamma}$. The details of the experiment are identical to those of the scheme in Fig. 1A with the exception that the carbonyl chemical shift of residue i (rather than the ^{15}N shift of residue i+1) is recorded during t_2. In this way cross and diagonal peaks at $[\omega_{C\gamma}(i),\omega_{C'}(i),\omega_{NH}(i+1)]$ and $[\omega_{C'}(i),\omega_{C'}(i),\omega_{NH}(i+1)]$ are obtained. Of course, in principle it is necessary to record only one of the two experiments listed in Fig. 1 to obtain the C'-C^{γ} couplings. However, for applications to either unfolded or partially folded protein states or to proteins with large amounts of spectral overlap it is often useful to record both spectra. In what follows we will refer to the experiments of Figs. 1A and B as HNCOC^{γ} and H(N)COC^{γ}, respectively, to distinguish the fact that the ^{15}N chemical shift is recorded in one but not the other.

As discussed in detail by Bax et al. (1994), it is the ratio of volume integrals of cross (V_C) and diagonal (V_D) peaks which is related to the coupling $J_{C'C\gamma}$ by the equation $V_C/V_D = -\tan^2(2\pi J_{C'C\gamma} T_C)$. However, if the line shapes of cross and diagonal peaks are identical the volume ratio can be replaced by the ratio of peak heights (Bax et al., 1994). In both of the experiments of Fig. 1 the line shapes of cross and diagonal peaks in F2 and F3 are the same and, because of the short acquisition time in t_1, the line shapes in this dimension are limited by digitization and to an excellent approximation are identical as well. The

values of $J_{C'C\gamma}$ can be derived, therefore, from the ratios of peak heights in these experiments.

Experiments for measuring $^3J_{NC\gamma}$

The pulse schemes in Fig. 2 illustrate the experiments that are performed to measure $J_{NC\gamma}$. Unlike the experiments for the measurement of $J_{C'C\gamma}$, where all of the information is present in a single data set, in this case separate experiments are recorded to obtain cross (HNC^{γ}) and diagonal peak (HNCO) intensities. For the HNC^{γ} experiment (Fig. 2A) the flow of magnetization can be described schematically as follows:

$$\begin{aligned} NH \xrightarrow{J_{NH}} {}^{15}N(t_1) \xrightarrow{J_{NC\gamma}} {}^{13}C^{\gamma}(t_2) \\ \xrightarrow{J_{NC\gamma}} {}^{15}N \xrightarrow{J_{NH}} NH(t_3) \end{aligned} \qquad (2)$$

where $J_{NC\gamma} = {}^3J_{NC\gamma}$, and Fourier transformation of the resultant data set gives rise to resonances (referred to as cross peaks) at $[\omega_N(i),\omega_{C\gamma}(i),\omega_{NH}(i)]$. The function describing the transfer of magnetization from ^{15}N to $^{13}C^{\gamma}$ is proportional to

$$\begin{aligned} &\exp(-2T_N/T_{2,N})\ \sin(2\pi J_{NC\gamma} T_N)\ \cos(2\pi J_{NC'} T_N) \\ &\times \prod_i \cos(2\pi J_{NC^i} T_N) \end{aligned} \qquad (3)$$

where $T_{2,N}$ is the ^{15}N transverse relaxation time, $J_{NC\gamma}$ is the three-bond ^{15}N-$^{13}C^{\gamma}$ coupling constant that we wish to measure, $J_{NC'}$ is the one-bond ^{15}N-$^{13}C'$ coupling, J_{NC^i} is the coupling between the ^{15}N spin and some other carbon coupling partner i (not the directly coupled $^{13}C'$) and $2T_N = T_N^a + T_N^b + T_N^c + T_N^d + 2T_N^e = T_N^f + T_N^g + 2T_N^h$ (see the legend to Fig. 2). Note that at this point in the discussion no distinction has been made between the relaxation rates of in-phase and antiphase ^{15}N magnetization components; this is deferred to the following section. Evolution of ^{15}N magnetization due to the one- and two-bond ^{15}N-$^{13}C^{\alpha}$ couplings during this period would significantly attenuate the signal and selective $^{13}C^{\alpha}$ inversion pulses are therefore inserted to refocus the effects of these couplings. It is essential that these pulses do not perturb $^{13}C^{\gamma}$ magnetization and in this regard 1.5 ms inversion pulses with the I-BURP-2 profile (Geen and Freeman, 1991) are employed, with a center of excitation at 57 ppm. Simulations indicate that magnetization between 57 ± 10 ppm is inverted to greater than 97.5% (500 MHz), while resonances upfield of 40 ppm and downfield of 74 ppm (all $^{13}C^{\gamma}$) are not affected (<2%). The $^{13}C^{\alpha}$ carbons of glycine residues are not properly inverted by this pulse and nitrogen magnetization of a residue immediately following a glycine will, therefore, evolve due to the two-bond $J_{NC\alpha}$ coupling. The exact evolution will be dependent on the effective flip angle of the $^{13}C^{\alpha}$ inversion pulses that perturb but do not completely invert the $^{13}C^{\alpha}$ of the glycine. Note that the same effect occurs for nitrogen magnetization which gives rise to the diagonal peak (see Fig. 2B) so that the ratio of intensities of cross and diagonal peaks for a residue following glycine is to an excellent approximation unaffected.

The HNC^{γ} experiment discussed above establishes connectivities between scalar-coupled ^{15}N and $^{13}C^{\gamma}$ spins, with a transfer function proportional to $\sin(2\pi J_{NC\gamma} T_N)$. The corresponding experiment which generates what will be referred to as diagonal peaks $[\cos(2\pi J_{NC\gamma} T_N)$ transfer function] is illustrated in Fig. 2B. In this case the flow of magnetization is given by

$$\begin{aligned} NH \xrightarrow{J_{NH}} {}^{15}N(t_1) \xrightarrow{J_{NC'}} {}^{13}C'(t_2) \\ \xrightarrow{J_{NC'}} {}^{15}N \xrightarrow{J_{NH}} NH(t_3) \end{aligned} \qquad (4)$$

and, in a manner analogous to more standard HNCO pulse schemes (Kay et al., 1990; Grzesiek and Bax, 1992), peaks at $[\omega_N(i),\omega_{C'}(i-1),\omega_{NH}(i)]$ are recorded. Note that the transfer function describing the flow of magnetization from ^{15}N to $^{13}C'$ is proportional to

$$\begin{aligned} &\exp(-2T_N/T_{2,N})\ \cos(2\pi J_{NC\gamma} T_N)\ \sin(\pi J_{NC'} T_N) \\ &\times \prod_i \cos(2\pi J_{NC^i} T_N) \end{aligned} \qquad (5)$$

with the same constant of proportionality as in Eq. 3.

Since in both the HNC^{γ} and HNCO experiments the magnetization is transferred from ^{15}N to either $^{13}C^{\gamma}$ or $^{13}C'$ and then back, the ratio of intensities of cross and diagonal peaks is given by

$$\tan^2(2\pi J_{NC\gamma} T_N)\ \cos^2(2\pi J_{NC'} T_N)/\sin^2(\pi J_{NC'} T_N) \qquad (6)$$

In order to maximize the sensitivity of each of the experiments, the delay $2T_N$ is set to $1/J_{NC'}$. Delaglio et al. (1991) have measured one-bond ^{15}N-$^{13}C'$ couplings in SNase and report average $J_{NC'}$ values of 14.8 ± 0.5 Hz for amino acids present in either α-helical or β-sheet conformations and 15.6 ± 0.5 Hz for residues in random coils. In the present set of experiments we have used a T_N delay corresponding to $J_{NC'} = 15$ Hz. For values of $J_{NC'}$ ranging from 14 to 16 Hz neglect of the terms related to $J_{NC'}$ in Eq. 6 results in an underestimate of $J_{NC\gamma}$ by less than 2%. However, in a number of cases in SNase the values of $J_{NC'}$ lie outside this range; the largest deviant is Lys^{78} for which $J_{NC'} = 13.1$ Hz is measured, and if the cosine and sine terms in Eq. 6 are neglected an error of ~6% in $J_{NC\gamma}$ is calculated in this case. However, the $\cos^2(2\pi J_{NC'} T_N)$ and $\sin^2(\pi J_{NC'} T_N)$ terms in Eq. 6 can be determined directly from the ratio of volumes of the one-bond N-C' cross peak in the HNC^{γ} experiment and the corresponding diagonal correlation peak in the HNCO experiment. Note that for the majority of residues in SNase $14\ \text{Hz} \le J_{NC'} \le 16$ Hz and the size of the N-C' correlation peak in the HNC^{γ} experiment is very small, indicating that $\cos^2(2\pi J_{NC'} T_N) \approx \sin^2(\pi J_{NC'} T_N) \approx 1$. The transfer of magnetization from ^{15}N to $^{13}C'$ in the HNC^{γ} scheme can be described by Eq. 3 with $J_{NC'}$ and

J_{NC^γ} interchanged. Therefore, the volume ratio of N-C' peaks in the HNC$^\gamma$ and HNCO experiments is given by

$$V_C/V_D = \sin^2(2\pi J_{NC'} T_N)/\sin^2(\pi J_{NC'} T_N) = 4\cos^2(\pi J_{NC'} T_N) \quad (7)$$

Although it is not possible to distinguish between the two values of $J_{NC'}$ which satisfy Eq. 7 (i.e., $J_{NC'} = (\pi T_N)^{-1} \cos^{-1}[\pm 0.5(V_C/V_D)^{0.5}]$) since both values are within the range of $J_{NC'}$ couplings that are observed in proteins, the required values of $\cos^2(2\pi J_{NC'} T_N)$ and $\sin^2(\pi J_{NC'} T_N)$ in Eq. 6 can nevertheless be obtained directly from the standard trigonometric identities, $\cos(2\pi J_{NC'} T_N) = \cos^2(\pi J_{NC'} T_N) - \sin^2(\pi J_{NC'} T_N)$ and $\sin^2(\pi J_{NC'} T_N) = 1 - \cos^2(\pi J_{NC'} T_N)$.

For both the HNC$^\gamma$ and HNCO experiments it is noteworthy that WURST adiabatic pulses (Kupce and Freeman, 1995) are applied at the centers of the $2T_N$ periods to invert all carbon spins. In the case of the HNC$^\gamma$ experiment this allows correlations to be established involving $^{13}C^\gamma$ spins of any residue. Although, in general, it is possible to record HNCO experiments with higher sensitivity by substituting the WURST pulses with C' selective inversion pulses, the use of broadband inversion schemes ensures that when the ratios of cross and diagonal peak intensities are calculated many of the passive couplings which are not of interest are canceled (see Eqs. 3 and 5).

In exceptional cases where all the peaks of interest are resolvable in a 2D ^{1}H-^{15}N correlation map, it is possible to record intensities of the diagonal peaks using the pulse scheme illustrated in Fig. 2A.1. In this case the ratio of cross and diagonal peak volumes is given by $\tan^2(2\pi J_{NC^\gamma} T_N)$. Unlike the experiments for the measurement of $J_{C'C^\gamma}$ where couplings can be obtained directly from the ratio of peak heights, accurate estimates of J_{NC^γ} values require the measurement of volume intensities. This is clear when (i) one considers that C$^\gamma$ and C' carbons have significantly different intrinsic line widths and that a longer t_2 acquisition time is recorded in the HNCO experiment relative to the HNC$^\gamma$ scheme; and (ii) in the case where a 2D ^{1}H-^{15}N correlation map is used to record diagonal peaks the intensities of cross and diagonal peaks are obtained from 3D and 2D spectra, respectively. Peak volumes can be measured by an iterative procedure in which the peaks are fit with model line shapes derived from the time domain. These model line shapes are generated from synthetic time domain data which are processed in exactly the same manner as the experimental data. The procedure provides a direct estimate of the first time domain point (i.e., peak volume). A second approach involves fitting the peaks with multidimensional Gaussian line shapes to get peak heights and line widths, and subsequently converting these parameters to volumes. The volumes are then scaled to account for the numbers of time domain points in each of the dimensions and for the estimated influence of the apodization functions used (Bax et al., 1994). Both procedures are accomplished in the elegant software package nmrPipe, written by Frank Delaglio, NIH (Delaglio et al., 1995).

A prerequisite for the accurate measurement of J_{NC^γ} values from two separate experiments (such as HNC$^\gamma$ and HNCO) is that the amount of starting magnetization (NH) in each experiment be identical. A potential complication arises from the fact that water magnetization is along the −z-axis at the start of the t_2 period and the different t_2 acquisition times that are employed in each of the experiments might well result in different levels of radiation damping and subsequently different steady-state values of water magnetization. This could lead to different levels of NH magnetization in each experiment for some of the residues, potentially complicating the extraction of quantitative J values. In order to minimize this problem a weak bipolar gradient pair is applied during t_2. In this way water magnetization, aligned along the −z-axis at the start of the t_2 period, remains along the −z-axis until the middle of the t_2 period when a ^{1}H 180° pulse restores the water to the +z-axis.

Although it is possible to develop experiments where both cross and diagonal sets of peaks are retained in the same data set (and we have done so), our preference is to separate N-C$^\gamma$ and N-C' peaks. This is extremely important in applications to proteins with significant amounts of spectral overlap. For example, J_{NC^γ} couplings could be measured from a single data set with diagonal and cross peaks recorded at $[\omega_N(i),\omega_N(i),\omega_{NH}(i)]$ and $[\omega_N(i),\omega_{C^\gamma}(i),$

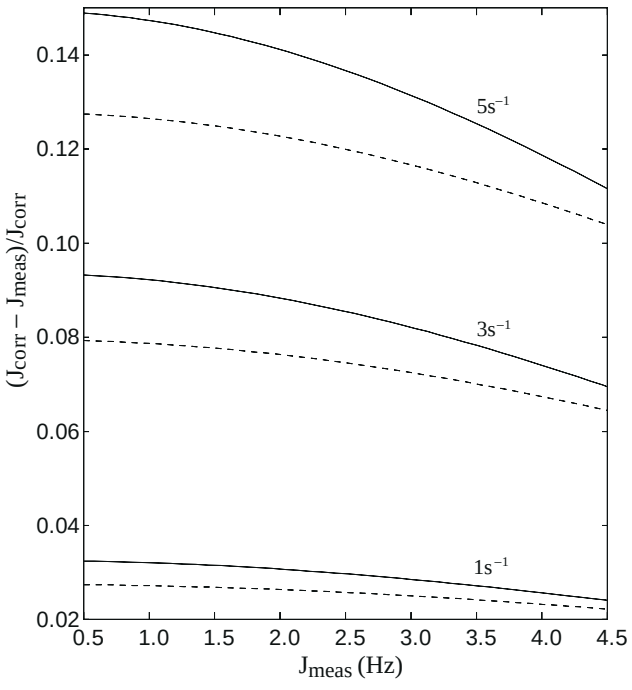

Fig. 3. Plots of the fractional error in measured J values, [J(correct) − J(measured)]/J(correct), as a function of the measured scalar coupling for different $^{13}C^\gamma$ spin flip rates. Values of $T_C = 28$ ms (dashed line) and $T_N = 33$ ms (solid line) are employed.

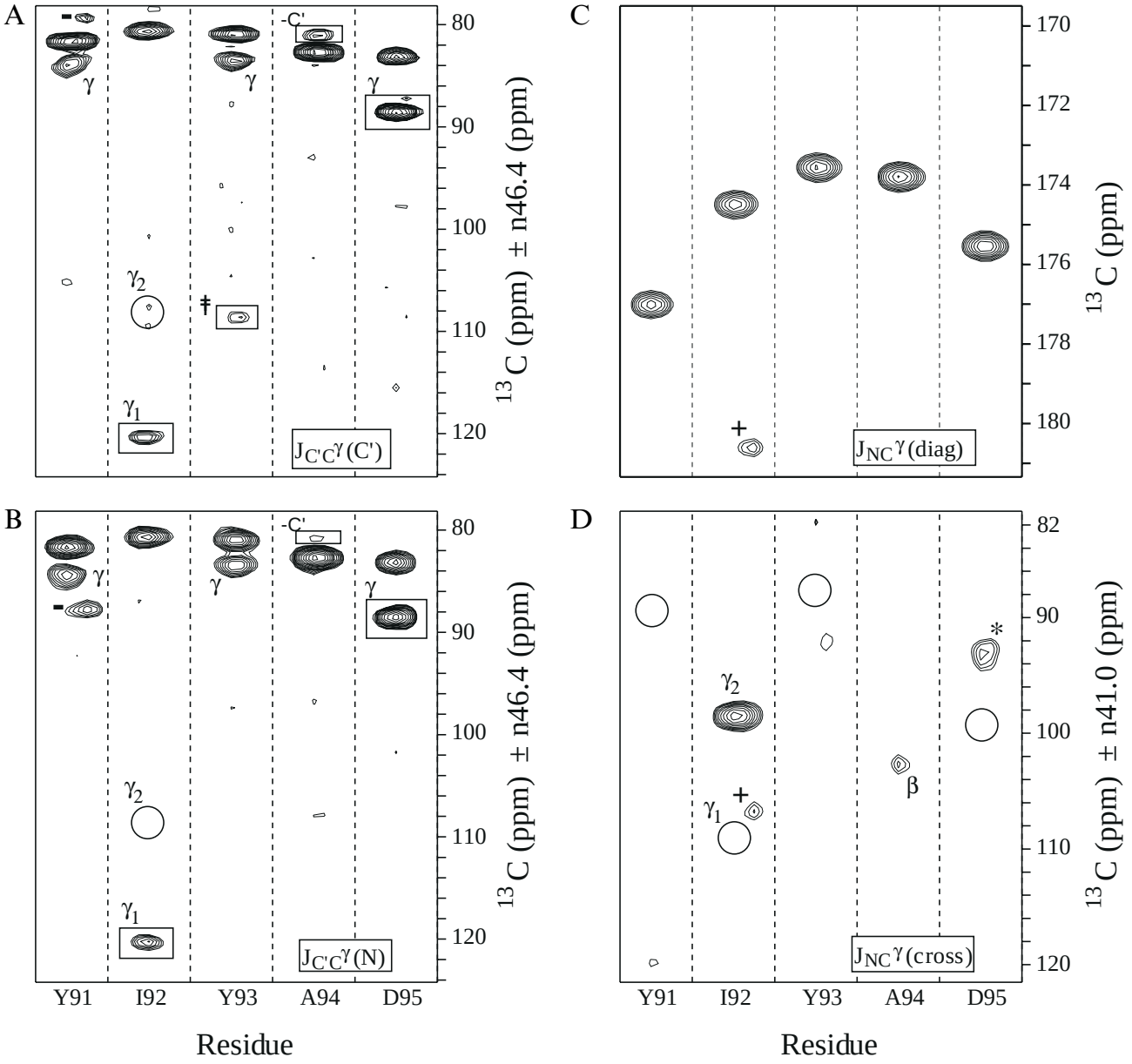

Fig. 4. Strip plots from H(N)COC$^{\gamma}$ (A), HNCOC$^{\gamma}$ (B), HNCO (C) and HNC$^{\gamma}$ (D) spectra, for residues Tyr^{91}–Asp^{95}. Positive and negative peaks are distinguished by placing boxes around peaks of opposite phase. Diagonal peaks are not marked, while correlation peaks to either C$^{\gamma}$ or C$^{\beta}$ are indicated by γ or β, respectively. Correlation peaks to the previous/next carbonyl are indicated by –C' or +C', respectively, while peaks denoted with + or – have increased intensity in an adjacent slice. Cross peaks labeled with ‡ are not assigned. Cross peaks indicated by * correspond to one-bond correlations arising from $J_{NC'}$, while the positions of expected cross peaks that are below the noise threshold are indicated by open circles. Note that different spectral widths were employed in the HNCOC$^{\gamma}$ class of experiments relative to HNC$^{\gamma}$. The value of n (see y-axis label) is an integer with $0 \le n \le 2$. The majority of the peaks have been aliased twice with $n = 2$ for the C' peaks and for many of the C$^{\gamma}$ (aliphatic) correlations. The notation $J_{C'C^{\gamma}}(x)$ indicates that C'-C$^{\gamma}$ couplings are measured from this experiment and that the spectrum is recorded with a constant-time x = (^{15}N,^{13}C') dimension, while $J_{NC^{\gamma}}$(cross)/$J_{NC^{\gamma}}$(diag) indicates that cross/diagonal peaks are obtained for measuring $J_{NC^{\gamma}}$ values.

$\omega_{NH}(i)$], respectively. The resolution for the diagonal peaks is, however, no better than that obtained in a 2D ^{1}H-^{15}N HSQC since two of the three chemical shifts are identical. This is similar to the situation described above in the context of measuring $J_{C'C^{\gamma}}$ couplings where diagonal peaks in one of the experiments are recorded at [$\omega_{C'}(i)$,$\omega_{C'}(i)$, $\omega_{NH}(i+1)$]. In this case an experiment with ^{15}N chemical shift evolution substituted for C' evolution is recorded to increase the number of residues for which couplings can be obtained in cases with significant overlap.

Finally, in addition to measuring three-bond $J_{NC^{\gamma}}$ couplings, it is also possible, in principle, to obtain three-bond $J_{NC^{\beta}}$ couplings from the HNC$^{\gamma}$, HNCO set of experiments through correlations linking the ^{15}N of residue i+1 with the C$^{\beta}$ of residue i (in HNC$^{\gamma}$), providing valuable information about ψ. Regrettably, the ^{13}C$^{\alpha}$ inversion pulses

applied during the periods in which ^{15}N magnetization evolves with respect to either $J_{NC\gamma}$ or $J_{NC\beta}$ (see above) perturb the C^{β} spins of threonine, serine, leucine, and in some cases phenylalanine, tyrosine and aspartic acid, and ψ values for these residues can therefore not be obtained using this method. Notably, we have not observed any three-bond N-C^{β} correlations in the protein systems that we have examined to date, suggesting that $^{3}J_{NC\beta}$ values are very small.

Relaxation effects

It is well known that in quantitative J-based experiments cross peaks can be attenuated relative to the corresponding diagonal peaks since antiphase magnetization which contributes to the intensity of the cross peaks relaxes more efficiently than in-phase signal from which the diagonal peaks are derived (Bax et al., 1994). Errors in the measured $J_{C'C\gamma}$ and $J_{NC\gamma}$ values can be corrected in a straightforward manner if the spin flip rate of the C^{γ} spin

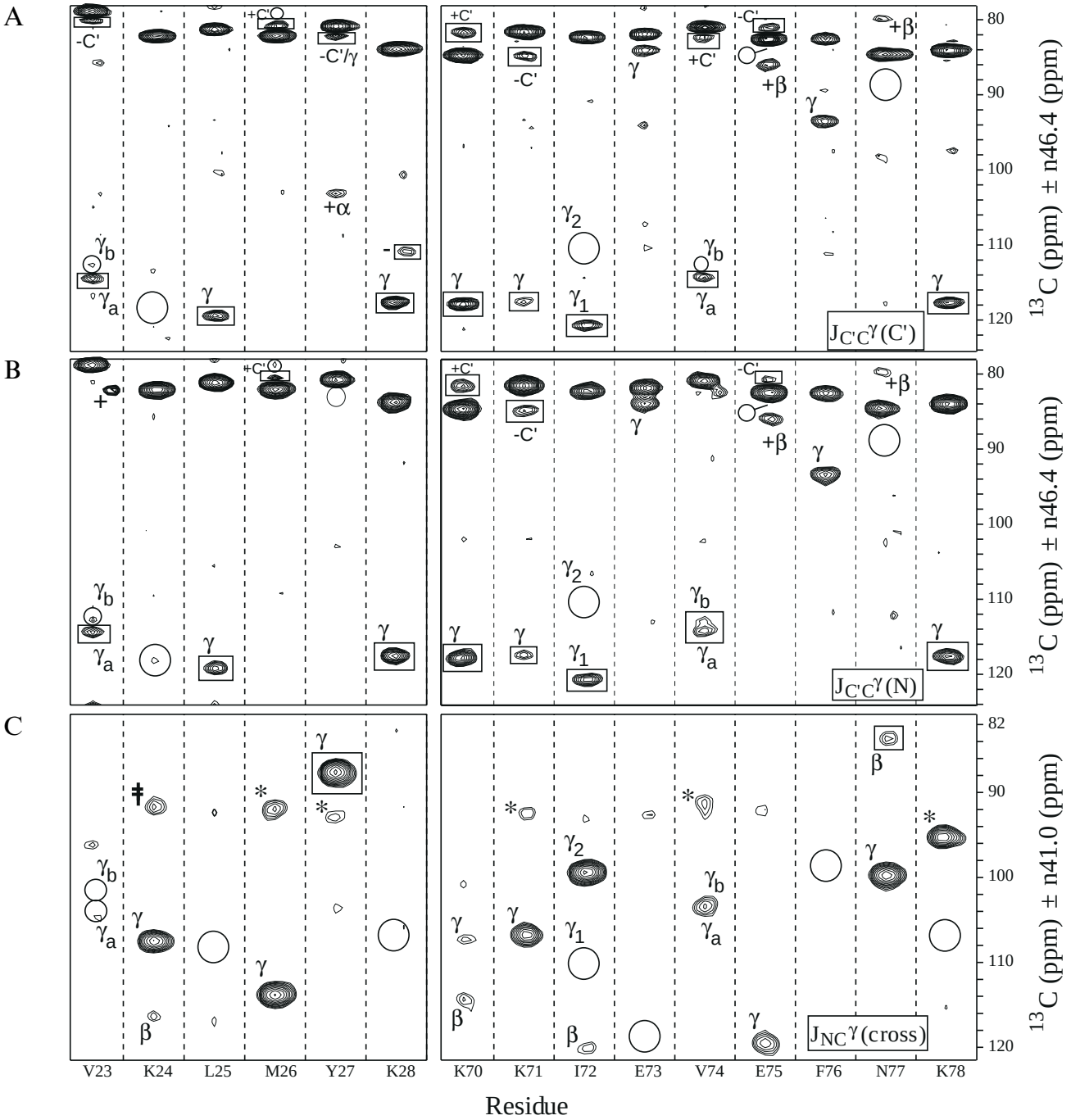

Fig. 5. Strip plots from H(N)COC$^{\gamma}$ (A), HNCOC$^{\gamma}$ (B) and HNC$^{\gamma}$ (C) spectra illustrating correlations for Val^{23}–Lys^{28} and Lys^{70}–Lys^{78}. Cross-peak notation is described in the legend to Fig. 4. In the case where stereospecific assignments of valine γ methyls are not available, the notation γ_a and γ_b is employed to distinguish the two methyl groups.

is known. The C^{γ} spin flip rate can be estimated from a number of different experiments. One straightforward approach is by recording a set of 2D ^{1}H-^{15}N correlation experiments in which magnetization of the form $N_zC_z^{\gamma}$ is created and allowed to relax for a variable period. The modification to the sequence of Fig. 2 for measuring the decay of $N_zC_z^{\gamma}$ is described in the legend to the figure. The flip rate of the C^{γ} spin $[1/T_1(C_z^{\gamma})]$ is well approximated by

$$1/T_1(C_z^{\gamma}) = 1/T_1(N_zC_z^{\gamma}) - 1/T_1(N_z) \quad (8)$$

where $1/T_1(N_zC_z^{\gamma})$ and $1/T_1(N_z)$ are the measured decay rates of $N_zC_z^{\gamma}$ two-spin order and longitudinal ^{15}N magnetization, respectively. Alternatively, $1/T_1(C_z^{\gamma})$ can be obtained by measuring the decay of $N_zC_z'C_z^{\gamma}$ longitudinal order established using a variant of the pulse scheme illustrated in Fig. 1A and subtracting the contributions from the C' and ^{15}N spin flips. Note that for the sizes of proteins currently studied by NMR, the one-bond ^{15}N-$^{13}C'$ couplings are much larger than the $^{13}C'$ spin flip rates and the correction of $J_{NC^{\gamma}}$ values obtained from the HNC^{γ} and HNCO experiments depends to an excellent approximation only on C^{γ} and not C' spin flip rates. Figure 3 illustrates the relation between values of $J_{C'C^{\gamma}}$ and $J_{NC^{\gamma}}$ that have been corrected for spin flip effects and measured (uncorrected) scalar coupling values as a function of different C^{γ} spin flip rates for values of T_C (Fig. 1) and T_N (Fig. 2) of 28 and 33 ms, respectively. For the case of CheY (14 kDa, correlation time of 7.1 ± 0.5 ns at 30 °C), we have measured an average C^{γ} spin flip rate of 3 ± 1 s^{-1} at 500 MHz and 30 °C, which suggests that on average, if uncorrected, coupling constant values are underestimated by 6–9% for this protein.

Applications to SNase

Figure 4 illustrates the quality of data that we have obtained from the experiments described above applied to a 1.5 mM sample of SNase complexed with Ca^{2+} and pdTp and uniformly enriched in ^{15}N and ^{13}C. A small region extending from Tyr^{91} to Asp^{95} is indicated, illustrating the cross and diagonal peaks in the $H(N)COC^{\gamma}$ (A) and $HNCOC^{\gamma}$ (B) experiments used to measure $J_{C'C^{\gamma}}$. The corresponding strips from the HNCO and HNC^{γ} experiments illustrate the diagonal (C) and cross (D) peaks, respectively, that are used to estimate $J_{NC^{\gamma}}$. The positions of expected cross peaks that are below the noise threshold are indicated with open circles. In the case of the $H(N)COC^{\gamma}$ and $HNCOC^{\gamma}$ experiments strips for a given residue are obtained at the NH shift of the succeeding amino acid, while for the HNCO and HNC^{γ} experiments strip plots at the NH and ^{15}N chemical shifts of a residue contain the N-C' and N-C^{γ} correlations of interest. On the basis of the $J_{C'C^{\gamma}}$ and $J_{NC^{\gamma}}$ couplings, χ_1 values of ~–60° are established for Tyr^{91}, Ile^{92}, Tyr^{93} and Asp^{95}. For all these residues $J_{C'C^{\gamma}}$ values (Ile γ_1) fall in the range of 2.9–3.3 Hz, with the exception of Asp^{95} for which a coupling of 5.1 Hz is measured. A strong N-C^{γ} correlation is observed for Ile^{92} (γ_2) from which a $J_{NC^{\gamma}2}$ coupling of –1.9 Hz is obtained. Note that for some residues additional peaks are observed such as the two-bond N-C^{β} correlation for Ala^{94} (Fig. 4D), a number of three-bond C'-C' correlations as well as a one-bond N-C' correlation for Asp^{95}. From the relative volumes of the N-C' correlation peaks in the HNC^{γ} and HNCO experiments, a $J_{NC'}$ value of either 14.1 or 16.2 Hz is calculated for Asp^{95} (see Eq. 7), in excellent agreement with the value (14.2 Hz) measured by Delaglio et al. (1991). Additional cross sections from the $H(N)COC^{\gamma}$ and $HNCOC^{\gamma}$ experiments as well as cross peaks from the HNC^{γ} experiment are illustrated in Fig. 5. Note the very strong correlation peak arising from the one-bond N-C' coupling for Lys^{78}; $J_{NC'} = 13.2$ or 17.2 Hz is calculated for this residue, which compares favorably with the value of 13.1 Hz measured by Delaglio et al. (1991).

Table 1 lists the values of $J_{C'C^{\gamma}}$ and $J_{NC^{\gamma}}$ couplings measured from experiments presented for the residues illustrated in Figs. 4 and 5 along with the corresponding

TABLE 1
VALUES OF $^{3}J_{C'C^{\gamma}}$ AND $^{3}J_{NC^{\gamma}}$ DETERMINED FOR THE SNase RESIDUES SHOWN IN FIGS. 4 AND 5[a]

Residue	$^{3}J_{C'C^{\gamma}}$ (Hz)	$^{3}J_{NC^{\gamma}}$ (Hz)	χ_1 (°)
Val^{23} (γ_a)	2.34 ± 0.13	<0.8	–47.4
Val^{23} (γ_b)	<1.5	<0.8	–47.4
Lys^{24}	<1.4	1.82 ± 0.04	–44.7
Leu^{25}	3.04 ± 0.10	<0.6	–52.9
Met^{26}	<1.3	2.13 ± 0.04	–173.1
Tyr^{27}	<1.4	2.17 ± 0.04	170.1
Lys^{28}	3.31 ± 0.06	<0.6	–69.8
Lys^{70}	2.90 ± 0.04	0.74 ± 0.09	–61.9
Lys^{71}	1.42 ± 0.15	1.21 ± 0.04	–51.5
Ile^{72} (γ_1)	3.11 ± 0.11	<0.5	–74.6
Ile^{72} (γ_2)	<1.7	2.07 ± 0.03	–74.6
Glu^{73}	3.40 ± 0.09	<0.6	–64.5
Val^{74} (γ_a)	2.61 ± 0.13	–[b]	–59.0
Val^{74} (γ_b)	2.03 ± 0.19	–[b]	–59.0
Glu^{75}	<1.5	1.37 ± 0.09	173.1
Phe^{76}	3.89 ± 0.12	<0.6	–71.6
Asn^{77}	<1.4	3.00 ± 0.05	–147.3
Lys^{78}	2.83 ± 0.06	<0.6	68.4
Tyr^{91}	2.95 ± 0.10	<0.68	–57.0
Ile^{92} (γ_1)	2.98 ± 0.12	<0.68	–65.2
Ile^{92} (γ_2)	<1.7	1.92 ± 0.05	–65.2
Tyr^{93}	3.37 ± 0.10	<0.7	–68.4
Asp^{95}	5.09 ± 0.07	<0.6	–57.0

[a] Values of $^{3}J_{C'C^{\gamma}}$ and $^{3}J_{NC^{\gamma}}$ were determined from the ratios of cross and diagonal peak intensities as described in the text. Values of χ_1 were extracted from the X-ray structure of SNase (Loll and Lattman, 1989; Protein Databank filename: 1snc). Maximum values of the unobserved couplings were determined from the ratio of the intensity of the smallest cross peak that was observable and the appropriate diagonal peak. The values of $^{3}J_{C'C^{\gamma}}$ and $^{3}J_{NC^{\gamma}}$ are not corrected for $^{13}C^{\gamma}$ spin flips.

[b] Not possible to measure due to overlap.

χ_1 values obtained from the X-ray-derived structure of ligated (Ca^{2+} and pdTp) SNase (Loll and Lattman, 1989). For many of the residues large $J_{C'C\gamma}$ couplings are accompanied by small $J_{NC\gamma}$ couplings and vice versa, consistent with a well-defined χ_1 rotameric state. Generally, the χ_1 values estimated on the basis of the NMR data and the values obtained from the crystal structure are in good agreement. However, a number of residues show differences in the solution and crystal forms of the protein. The values of $J_{C'C\gamma}$ and $J_{NC\gamma}$ measured for Lys^{71} and Val^{74} suggest rotamer averaging or the adoption of noncanonical χ_1 angles, while the χ_1 values determined from the X-ray structure indicate defined rotameric states for these residues. In addition, the measured $J_{NC\gamma}$ value for Glu^{75} (1.4 Hz) is not consistent with a χ_1 value of 173° obtained from the X-ray-derived structure of SNase. The coupling data for Lys^{24} and Lys^{78} indicate χ_1 values of ≈180° and ≈−60°, respectively, while χ_1 values of −45° and 68° are obtained from the X-ray structure. It is noteworthy that both of these residues are near the surface of the protein and that in the structure of unligated SNase (Hynes and Fox, 1991) χ_1 values of −165° and −63° are obtained for Lys^{24} and Lys^{78}, respectively. Finally, the $C'C^{\gamma}$ coupling constant measured for Val^{23} is consistent with averaging within the $\chi_1 = -60°$ well; a χ_1 value of −47° is obtained for Val^{23} from the crystal structure.

Conclusions

A number of pulse schemes are presented for the measurement of three-bond $J_{C'C\gamma}$ and $J_{NC\gamma}$ couplings. Correlations for aromatic amino acids, Asx and aliphatic residues are obtained in each of these experiments allowing the measurement of $J_{C'C\gamma}$ and $J_{NC\gamma}$ values for all C^{γ} containing residues. The combination of $J_{C'C\gamma}$ and $J_{NC\gamma}$ couplings facilitates the assignment of χ_1 rotamers in the case of well-defined states. In addition, in the case of unfolded or partially folded protein states, the measurement of these J values will provide important information to supplement NOEs for the characterization of residual structure in such systems.

Acknowledgements

We thank Drs. Dennis Torchia, NIH, and Dave Shortle, Johns Hopkins University, for the generous gifts of samples of SNase used in the present study and Frank Delaglio, NIH, for kindly making available software for analysis prior to publication and assisting with data analysis. This work was supported by grants from the Natural Sciences and Engineering Research Council of Canada and the Medical Research Council of Canada. N.A.F. is a research fellow of the National Cancer Institute of Canada supported with funds provided by the Terry Fox Run.

References

Archer, S.J., Ikura, M., Torchia, D.A. and Bax, A. (1991) *J. Magn. Reson.*, **95**, 636–641.

Bax, A. and Grzesiek, S. (1993) *Acc. Chem. Res.*, **26**, 131–138.

Bax, A., Vuister, G.W., Grzesiek, S., Delaglio, F., Wang, A.C., Tschudin, R. and Zhu, G. (1994) *Methods Enzymol.*, **239**, 79–105.

Biamonti, C., Rios, C.B., Lyons, B.A. and Montelione, G. (1994) *Adv. Biophys. Chem.*, **4**, 51–120.

Bohlen, J.-M., Rey, M. and Bodenhausen, G. (1989) *J. Magn. Reson.*, **84**, 191–197.

Boyd, J. and Soffe, N. (1989) *J. Magn. Reson.*, **85**, 406–413.

Bystrov, V.F. (1976) *Prog. NMR Spectrosc.*, **10**, 41–81.

Clore, G.M. and Gronenborn, A.M. (1991) *Science*, **252**, 1390–1399.

Delaglio, F., Torchia, D.A. and Bax, A. (1991) *J. Biomol. NMR*, **1**, 439–446.

Delaglio, F., Grzesiek, S., Vuister, G.W., Zhu, G., Pfeifer, J. and Bax, A. (1995) *J. Biomol. NMR*, **6**, 277–293.

Eggenberger, U., Karimi-Nejad, Y., Thuring, H., Rüterjans, H. and Griesinger, C. (1992) *J. Biomol. NMR*, **2**, 583–590.

Emerson, S.D. and Montelione, G.T. (1992) *J. Am. Chem. Soc.*, **114**, 354–356.

Emsley, L. and Bodenhausen, G. (1992) *J. Magn. Reson.*, **97**, 135–148.

Ernst, E.E., Bodenhausen, G. and Wokaun, A. (1987) *Principles of Nuclear Magnetic Resonance in One and Two Dimensions*, Oxford University Press, Oxford, U.K.

Geen, H. and Freeman, R. (1991) *J. Magn. Reson.*, **93**, 93–141.

Griesinger, C., Sørensen, O.W. and Ernst, R.R. (1986) *J. Chem. Phys.*, **85**, 6837–6843.

Grzesiek, S. and Bax, A. (1992) *J. Magn. Reson.*, **96**, 432–440.

Grzesiek, S., Ikura, M., Clore, G.M., Gronenborn, A. and Bax, A. (1992) *J. Magn. Reson.*, **96**, 215–221.

Grzesiek, S. and Bax, A. (1993) *J. Am. Chem. Soc.*, **115**, 12593–12594.

Grzesiek, S., Kuboniwa, H., Hinck, A.P. and Bax, A. (1995) *J. Am. Chem. Soc.*, **117**, 5312–5315.

Harbison, G.J. (1993) *J. Am. Chem. Soc.*, **115**, 3026–3027.

Hu, J.-S. and Bax, A. (1996) *J. Am. Chem. Soc.*, **118**, 8170–8171.

Hynes, T.R. and Fox, R.O. (1991) *Proteins*, **10**, 92–105.

Karimi-Nejad, Y., Schmidt, J.M., Rüterjans, H., Schwalbe, H. and Griesinger, C. (1994) *Biochemistry*, **33**, 5481–5492.

Karplus, M. (1959) *J. Chem. Phys.*, **30**, 11–15.

Kay, L.E., Ikura, M., Tschudin, R. and Bax, A. (1990) *J. Magn. Reson.*, **89**, 496–514.

Kay, L.E., Keiffer, P. and Saarinen, T. (1992) *J. Am. Chem. Soc.*, **114**, 10663–10665.

Kay, L.E. (1993) *J. Am. Chem. Soc.*, **115**, 2055–2057.

Kupce, E. and Freeman, R. (1995) *J. Magn. Reson.*, **A115**, 273–276.

Loll, P.J. and Lattman, E.E. (1989) *Proteins Struct. Funct. Genet.*, **5**, 183–201.

Marion, D., Ikura, M. and Bax, A. (1989a) *J. Magn. Reson.*, **84**, 425–430.

Marion, D., Ikura, M., Tschudin, R. and Bax, A. (1989b) *J. Magn. Reson.*, **85**, 393–399.

McCoy, M.A. and Mueller, L. (1992) *J. Am. Chem. Soc.*, **114**, 2108–2112.

Morris, G.A. and Freeman, R. (1979) *J. Am. Chem. Soc.*, **101**, 760–761.

Nicholson, L.K., Kay, L.E., Baldisseri, D.M., Arango, J., Young, P.E., Bax, A. and Torchia, D.A. (1992) *Biochemistry*, **31**, 5253–5263.

Patt, S. (1992) *J. Magn. Reson.*, **96**, 94–102.
Piotto, M., Saudek, V. and Sklenář, V. (1992) *J. Biomol. NMR*, **2**, 661–665.
Schmidt, J.M., Löhr, F. and Rüterjans, H. (1996) *J. Biomol. NMR*, **7**, 142–152.
Schwalbe, H., Rexroth, A., Eggenberger, U., Geppert, T. and Griesinger, C. (1993) *J. Am. Chem. Soc.*, **115**, 7878–7879.
Shaka, A.J., Keeler, J., Frenkiel, T. and Freeman, R. (1983) *J. Magn. Reson.*, **52**, 335–338.
Sørensen, O.W., Eich, G.W., Levitt, M.H., Bodenhausen, G. and Ernst, R.R. (1983) *Prog. NMR Spectrosc.*, **16**, 163–192.
Van de Ven, F.J.M. (1995) *Multidimensional NMR in Liquids*, VCH, New York, NY, U.S.A.
Vuister, G.W. and Bax, A. (1993) *J. Am. Chem. Soc.*, **115**, 7772–7777.
Vuister, G.W., Wang, A.C. and Bax, A. (1993) *J. Am. Chem. Soc.*, **115**, 5334–5335.
Wang, A.C. and Bax, A. (1995) *J. Am. Chem. Soc.*, **117**, 1810–1813.
Wüthrich, K. (1986) *NMR of Proteins*, Wiley, New York, NY, U.S.A.
Zhang, O. and Forman-Kay, J.D. (1995) *Biochemistry*, **34**, 6784–6794.
Zhang, O., Forman-Kay, J.D., Shortle, D. and Kay, L.E. (1997) *J. Biomol. NMR*, **9**, 181–200.
Zhu, G. and Bax, A. (1990) *J. Magn. Reson.*, **90**, 405–410.

Appendix

Effect of finite B_1 field strength on measured C'-C$^\gamma$ couplings

Figure 1A illustrates a pulse scheme for the measurement of $J_{C'C^\gamma}$ where the coupling constant is obtained from the relative intensities of diagonal peaks at ($\omega_{C'}$,ω_N, ω_{NH}) and cross peaks at (ω_{C^γ},ω_N,ω_{NH}), as described in the text. Quadrature in t_1 is obtained by recording two sets of spectra for each t_1 value, where in the second set the phases of the rf pulses denoted by $\phi2$, $\phi3$ and $\phi4$ in Fig. 1A are incremented by $\pi/2$. Note that the carbon pulses of phases $\phi4$ and $\phi5$ are applied at 101 ppm, approximately equidistant from the chemical shifts of the carbonyl spins and many of the C$^\gamma$ spins. Because the offset is no longer negligible with respect to the rf field strength (see below), it is important to establish that the off-resonance effects of these two pulses (phases $\phi4$ and $\phi5$) do not compromise the accuracy of the measured scalar couplings. Note that all the other carbon pulses in the sequence can be considered as 'on-resonance'.

The application of a pulse with flip angle β, phase ϕ and tilt angle θ from the z-axis is readily described using product operators (Ernst et al., 1987; Van de Ven, 1995) via

$$\mathbf{I} \xrightarrow{\beta,\theta,\phi} \mathbf{AI} \tag{A1}$$

where **I** is a column vector with elements

$$\mathbf{I} = \begin{pmatrix} I_z \\ I_x \\ I_y \end{pmatrix} \tag{A2}$$

where I_j, $j = (z,x,y)$, is the j-component of magnetization and **A** is a 3×3 matrix listing the coefficients of I which describe how magnetization is transformed by the pulse; for example $I_z \rightarrow A_{11} I_z + A_{12} I_x + A_{13} I_y$. The elements of A $\{A_{ij}: 1 \le i \le 3, 1 \le j \le 3\}$ are given in Sørensen et al. (1983) with β and θ defined according to

$$\beta = -\gamma\tau_p(B_1^2 + \Delta B_0^2)^{0.5} \text{ and } \theta = \arctan(B_1/\Delta B_0) \tag{A3}$$

where γ is the gyromagnetic ratio of the spin, τ_p is the pulse width, $\gamma B_1/(2\pi)$ is the B_1 field strength in Hz and $\gamma\Delta B_0/(2\pi)$ is the offset of the spin from the carrier, also in Hz. [For example, $A_{12} = \sin(\beta)\sin(\phi)\sin(\theta) + \sin^2(\beta/2)\cos(\phi)\sin(2\theta)$.] When pulses are applied along the ±x-axes or along the ±y-axes, the value ϕ is set to 0° (x), 180° (–x) or ±90° (±y), respectively, in the expressions describing the elements of **A**. In what follows, the elements of **A** for which $\phi = 0°$ are denoted by b_{ij} (x pulse), while the elements of **A** for which $\phi = 90°$ (y pulse) are described by a_{ij}.

For the case of $\phi2 = \phi3 = x$, $\phi4 = \pm y$, a product operator calculation, neglecting the effects of relaxation as well as any multiplicative factors that are in expressions for both the diagonal and cross peak intensities, retaining only those terms not suppressed by the phase cycling, and assuming that the ^{15}N 180° pulse in the center of the t_1 period is instantaneous, shows that the signal for the diagonal peak is given by

$$\begin{aligned} &\cos^2(2\pi J_{C'C^\gamma} T_C)\,(A_1^2 + B_1^2)^{0.5} \cos(\omega_{C'} t_1 + \alpha_1) \\ &+ \sin^2(2\pi J_{C'C^\gamma} T_C)\,(A_2^2 + B_2^2)^{0.5} \cos(\omega_{C'} t_1 + \alpha_2) \end{aligned} \tag{A4}$$

where

$$\begin{aligned} A_1 &= a'_{23}a'_{32} + (a'_{33})^2, \\ B_1 &= -a'_{23}a'_{33} + a'_{33}a'_{32} \end{aligned} \tag{A4a}$$

$$\begin{aligned} A_2 &= -(a'_{22}a_{11})^2 + (a'_{32})^2(a_{11})^2, \\ B_2 &= a'_{22}a'_{23}(a_{11})^2 - a'_{32}a'_{22}(a_{11})^2 \end{aligned} \tag{A4b}$$

and

$$\begin{aligned} \tan(\alpha_i) &= (-B_i/A_i), \\ \cos(\alpha_i) &= A_i/(A_i^2 + B_i^2)^{0.5}, \\ \sin(\alpha_i) &= -B_i/(A_i^2 + B_i^2)^{0.5}, \\ i &= 1,2 \end{aligned} \tag{A4c}$$

Note that in the expressions listed above a'_{ij} denotes the ijth element in **A** for the C' spin, while a_{ij} is the corre-

sponding element in matrix **A** for the C^{γ} spin. The signal for the cross peak is given by

$$-\sin^2(2\pi J_{C'C^{\gamma}} T_C)\,(A_3^2 + B_3^2)^{0.5}\cos(\omega_{C^{\gamma}} t_1 + \alpha_3) \quad \text{(A5)}$$

where

$$\begin{aligned} A_3 &= -(a'_{12})^2(a_{12})^2 + (a'_{12})^2(a_{13})^2, \\ B_3 &= -(a'_{12})^2 a_{21} a_{13} + (a'_{12})^2 a_{31} a_{12} \end{aligned} \quad \text{(A5a)}$$

and

$$\begin{aligned} \tan(\alpha_3) &= (-B_3/A_3), \\ \cos(\alpha_3) &= -A_3/(A_3^2 + B_3^2)^{0.5}, \\ \sin(\alpha_3) &= B_3/(A_3^2 + B_3^2)^{0.5} \end{aligned} \quad \text{(A5b)}$$

The first term in Eq. A4 arises from in-phase magnetization which resides on the C' spin for both of the $2T_C$ periods in the sequence. In contrast, the second term originates from C' magnetization (C'_y) which evolves into $2C'_xC^{\gamma}_z$ via $J_{C'C^{\gamma}}$ during the first $2T_C$ period. Because of off-resonance effects, a fraction of this magnetization is not affected by either of the pulses flanking the t_1 period and therefore this signal evolves at the carbonyl frequency in t_1. This magnetization is refocused into C'_y during the subsequent delay $2T_C$. Finally, it should be noted that for the offsets and rf field strengths in the present experiment (see below) the phase α_i (or β_i, see below) is linearly dependent on the chemical shift offset of the appropriate C^{γ} or C' spin and is well approximated by the expression

$$\alpha_i = 8\tau_p \Delta\nu_0,\ \Delta\nu_0 = \gamma\Delta B_0/(2\pi) \quad \text{(A6)}$$

The relevant terms for the signals contributing to the diagonal peaks in the case of $\phi2 = \phi3 = y$, $\phi4 = \pm x$ are given by

$$\begin{aligned} &\cos^2(2\pi J_{C'C^{\gamma}} T_C)\,(C_1^2 + D_1^2)^{0.5}\sin(\omega_{C'} t_1 + \beta_1) \\ &+ \sin^2(2\pi J_{C'C^{\gamma}} T_C)\,(C_2^2 + D_2^2)^{0.5}\sin(\omega_{C'} t_1 + \beta_2) \end{aligned} \quad \text{(A7)}$$

where

$$\begin{aligned} C_1 &= a'_{23}b'_{22} + a'_{33}b'_{23}, \\ D_1 &= -a'_{23}b'_{23} + a'_{33}b'_{22} \end{aligned} \quad \text{(A7a)}$$

$$\begin{aligned} C_2 &= a'_{22}a_{11}b'_{32}b_{11} + a'_{32}a_{11}b'_{33}b_{11}, \\ D_2 &= -a'_{22}a_{11}b'_{33}b_{11} + a'_{32}a_{11}b'_{32}b_{11} \end{aligned} \quad \text{(A7b)}$$

and

$$\begin{aligned} \tan(\beta_i) &= (C_i/D_i), \\ \cos(\beta_i) &= D_i/(C_i^2 + D_i^2)^{0.5}, \\ \sin(\beta_i) &= C_i/(C_i^2 + D_i^2)^{0.5}, \\ i &= 1,2 \end{aligned} \quad \text{(A7c)}$$

In this case the signal from which the cross peak arises is given by

$$-\sin^2(2\pi J_{C'C^{\gamma}} T_C)\,(C_3^2 + D_3^2)^{0.5}\sin(\omega_{C^{\gamma}} t_1 + \beta_3) \quad \text{(A8)}$$

where

$$\begin{aligned} C_3 &= a'_{12}a_{21}b'_{31}b_{12} + a'_{12}a_{31}b'_{31}b_{13}, \\ D_3 &= -a'_{12}a_{21}b'_{31}b_{13} + a'_{12}a_{31}b'_{31}b_{12} \end{aligned} \quad \text{(A8a)}$$

and

$$\begin{aligned} \tan(\beta_3) &= (C_3/D_3), \\ \cos(\beta_3) &= -D_3/(C_3^2 + D_3^2)^{0.5}, \\ \sin(\beta_3) &= -C_3/(C_3^2 + D_3^2)^{0.5} \end{aligned} \quad \text{(A8b)}$$

In these expressions we have neglected the effects of relaxation, have included only those terms that do not get canceled by the phase cycling and have omitted any factors that appear for both cross and diagonal peaks.

Insight into the effects of these off-resonance pulses can be obtained by considering a numerical example. For the carrier positioned at 101 ppm, assuming C' and C^{γ} spins at 175 and 27 ppm, respectively (i.e., the carrier is placed in between the two coupled spins), a τ_p of 12 μs (90° pulse) and for the case of $\phi2 = \phi3 = x$, $\phi4 = \pm y$, the signal of interest is given by

$$\begin{aligned} &\cos^2(2\pi J_{C'C^{\gamma}} T_C)\ 0.8184\cos(\omega_{C'} t_1 - 0.9206) \\ &+ \sin^2(2\pi J_{C'C^{\gamma}} T_C)\ 0.000319\cos(\omega_{C'} t_1 - 0.7047) \end{aligned} \quad \text{(A9)}$$

for the diagonal peak and

$$-\sin^2(2\pi J_{C'C^{\gamma}} T_C)\ 0.8152\cos(\omega_{C^{\gamma}} t_1 + 0.8813) \quad \text{(A10)}$$

for the cross peak. For the case of $\phi2 = \phi3 = y$, $\phi4 = \pm x$, the signal is identical, with the exception that the $\cos(\omega_C t_1 + \theta)$ terms are replaced by $\sin(\omega_C t_1 + \theta)$. Note that the term that contributes to the diagonal peak and that is proportional to $\sin^2(2\pi J_{C'C^{\gamma}} T_C)$ is more than 3 orders of magnitude smaller than the term proportional to $\cos^2(2\pi J_{C'C^{\gamma}} T_C)$ and can be ignored. A second point of interest is that the absolute values of the phases of the cross and diagonal terms differ by 2.25°. (Note that the phases are of opposite signs since the C' and C^{γ} spins are on different sides of the carbon carrier.) Rewriting Eq. A10 as

$$\begin{aligned} &-\sin^2(2\pi J_{C'C^{\gamma}} T_C)\ 0.8152\cos(\omega_{C^{\gamma}} t_1 + 0.8813) = \\ &-\sin^2(2\pi J_{C'C^{\gamma}} T_C)\ 0.8152\cos(\omega_{C^{\gamma}} t_1 + 0.9206) \\ &-\sin^2(2\pi J_{C'C^{\gamma}} T_C)\ 0.0320\cos(\omega_{C^{\gamma}} t_1 - 0.6685) \end{aligned} \quad \text{(A11)}$$

indicates that this phase difference introduces a negligible error as the second term on the right-hand side of Eq. A11 is a factor of 15 smaller than the first term and approximately 90° out of phase. Finally, and perhaps most

significantly, the intensities of both cross and diagonal peaks are attenuated relative to the case where $B_1 \rightarrow \infty$ by very similar amounts (0.818 versus 0.815) so that the ratio of peaks (and hence the measured scalar coupling value) is unaffected.

Numerical simulations have been performed with a number of different C^{γ} offsets to ensure that, for carbon rf strengths available on modern commercial probes and for typical C^{γ} offsets (at 500, 600 MHz), the errors introduced by off-resonance pulses are very small. However, this does not mean that such effects can always be neglected. Simulations with a B_1 field strength on the order of the $^{13}C^{\gamma}$ chemical shift offset establish that errors of significance are introduced. Specifically, in this case it is not even possible to phase cross and diagonal peaks. Therefore, care must be taken in these experiments to ensure that the rf field used for carbon pulses is the highest possible.